Electronic Supplementary Information

High-performance electrocatalytic nitrate reduction to ammonia enabled by a copper-porphyrin-based porous aromatic framework

Shan Zhang,[a] Yanni Peng,[a] Hongming He,[*a,b] Yingying Zhu,[a] Chun Chen,[a] Shuting Du,[*a] Cheng-Peng Li,[*a] Xiao Liang,[*b] and Quanshun Li,[*b]

[a] *College of Chemistry, Academy of Interdisciplinary Studies on Intelligent Molecules, Tianjin Key Laboratory of Structure and Performance for Functional Molecules, Tianjin Normal University, Tianjin 300387, P. R. China.*

[b] *Key Laboratory for Molecular Enzymology and Engineering of Ministry of Education, School of Life Sciences, Jilin University, Changchun 130012, P. R. China.*

Chem. Commun.

1. Experimental Detail

Material and general method. Chemicals and solvents were obtained through commercial purchase. Pyrrole (99%), sodium hypochlorite (NaClO, 6~14% active chlorine basis), Nessler (98%), and ferric chloride ($FeCl_3$, 99%) were obtained from Maclin Co., Ltd. Anhydrous sodium sulfate (Na_2SO_4, 99%) and potassium bromide (KBr, 99%) were obtained from J&K Scientific Co., Ltd. Copper(II) acetate ($Cu(OAc)_2$, 98%) was acquired from Tianjin Heowns Co., Ltd. Sodium nitrate ($NaNO_3$, 99%) and sodium nitrite ($NaNO_2$, 99%) were purchased from Tianjin Damao Co., Ltd. Ammonium chloride (NH_4Cl, 99.99%), $^{15}NH_4Cl$ (99 atom%), $Na^{15}NO_3$ (99 atom%), sulfamic acid (99%), p-aminobenzenesulfonamide (99%), N-(1-Naphthyl) ethylenediamine dihydrochloride (98%), sodium citrate ($Na_3C_6H_5O_7 \cdot 2H_2O$, 99.5%) and sodium hydroxide (NaOH, 98%) were obtained from Aladdin Co., Ltd. Hydrazine hydrate (N_2H_4, 5% HCl) was obtained from Guobiao (Beijing) Testing and Certification, Co., Ltd. Nitric acid (HNO_3, 99.8%) was obtained from Tianjin Yuanli Chemical Co., Ltd. Ethanol (EtOH, AR) and methanol (MeOH, AR) were purchased from Shandong Bocheng Chemical Co., Ltd. Dichloromethane (CH_2Cl_2, AR), trichloromethane ($CHCl_3$, AR), hydrochloric acid (HCl, 36~38%) and isopropanol (AR) were obtained from Tianjin Fengchuan Chemical Reagent Co., Ltd. N,N-dimethylformamide (DMF, AR), ethyl acetate (AR), sodium nitroprusside ($C_5H_4FeN_6Na_2O_3$, 98.5%), salicylic acid ($C_7H_6O_3$, 99.5%), 4-(9-carbazolyl)benzaldehyde ($C_{19}H_{13}NO$, 95%), boron trifluoride diethyl etherate ($C_4H_{10}BF_3O$, 98%) and para-(dimethylamino) benzaldehyde ($C_9H_{11}NO$, AR) were purchased from Kaimat (Tianjin) Chemical Technology Co., Ltd. High-purity Ar (99.999%) was purchased from Huanyu Co., Ltd.

Fourier transform infrared (FT-IR) spectra were collected on a Bruker ALPHA-T FT-IR spectrometer. Powder X-ray diffraction (PXRD) patterns were measured on a

Haoyuan·DX-2700BH. The morphology and microstructure were carried out on a Nova Nano SEM 230 scanning electron microscope (SEM) and Tecnai G^2 F20 S-TWIN transmission electron microscope (TEM). X-ray photoelectron spectra (XPS) were carried out on an AXIS Ultra DLD X-ray photoelectron spectroscopy. Ultraviolet-visible (UV-vis) spectra were recorded on Mapada V-1200 spectrometer. ^{1}H nuclear magnetic resonance (NMR) spectra were conducted on Bruker AV 400 spectrometer. Electrochemical experiments were carried out on CHI760E electrochemical workstation. Inductively coupled plasma optical emission spectrometry (ICP-OES) was measured on Thermo Scientific iCAP 6500 system.

2. Synthesis

Synthesis of tetrakis(carbazol-9-ylphenyl)porphyrin (TCPP)[1]

To a mixture of 4-(9-carbazolyl)benzaldehyde (2.6 g, 10 mmol) and pyrrole (0.67 g, 10 mmol) in dichloromethane (75 mL) at room temperature was added boron trifluoride etherate (0.4 mL) with stirring. After the mixture was stirred for 2 h, p-chloranil (2.2 g, 8.8 mmol) was added and the resulting mixture was allowed to stir for 30 min at room temperature. The solvent was removed under reduced pressure, and the residue was chromatographed over silica gel using dichloromethane as the eluent. The obtained product was dissolved in dichloromethane and precipitated with methanol, yielding a purple solid (40% yield). ^{1}H NMR (600 MHz, $CDCl_3$) δ 8.91 (d, J = 8.1 Hz, 8H), 8.80 (s, 8H), 8.34 (d, J = 8.1 Hz, 8H), 8.29 (d, J = 7.9 Hz, 8H), 7.94 (d, J = 8.2 Hz, 8H), 7.62 (t, J = 7.6 Hz, 8H), 7.46 (t, J = 5.7 Hz, 8H).

Synthesis of CuTCPP

Add TCPP (0.256 g, 0.2 mmol) to a three necked flask containing DMF (50 mL), heat and reflux at 100 ºC under N_2 atmosphere for 1 h. Dissolve $Cu(OAc)_2$ (0.055g, 0.3 mmol) in DMF (5 mL), then inject it into the three necked flask and continue to heat and reflux at

100 ºC under N_2 atmosphere for 2 h. After the reaction is complete, cool to room temperature, add 50 mL of deionized water, adjust the pH of the solution to 8-9 with ammonia water to precipitate, filter and wash with deionized water, and vacuum dry at 80 ºC for 12 h.

Synthesis of TCPP-PAF[2]

The solution of anhydrous chloroform (60 mL) with TCPP (0.402 g, 0.3 mmol) was bubble with N_2 for 30 min. Next, a suspension of $FeCl_3$ (2.19 g, 13.5 mmol) in anhydrous chloroform (15 mL) was added dropwise to the TCPP solution under N_2 atmosphere. The resulting mixture was magnetically stirred for 3 days under N_2 at room temperature. Then, methanol (100 mL) was added to the mixture, and stirred for 1 h, and the solid was gathered by percolation and washed with methanol. The collected solid was stirred acutely in HCl solution (37%) for 2 h. The solid was collected by filtration and washed with methanol and water. The obtained solid was extracted in a Soxhlet extractor with methanol and tetrahydrofuran for 24 h, respectively. The collected solid was dried in a vacuum oven at 100 ºC overnight (yield: 95%).

Synthesis of CuTCPP-PAF

Add TCPP-PAF (150 mg) to a three necked flask containing DMF (50 mL), heat and reflux at 100 ºC under N_2 atmosphere for 1 h. Dissolve $Cu(OAc)_2$ (0.036 g, 0.2 mmol) in DMF (5 mL), then inject it into the three necked flask and continue to heat and reflux at 100 ºC under N_2 atmosphere for 2 h. After the reaction is complete, cool to room temperature, add 50 mL of deionized water, adjust the pH of the solution to 8-9 with ammonia water to precipitate, filter and wash with deionized water, and vacuum dry at 80 ºC for 12 h.

3. Preparation of Working Electrodes

Catalysts (5.0 mg) were dispersed in a mixed solution of isopropanol/Nafion (1.0 mL, V:V

= 950:50) and ultrasonicated for 1 h to generate a homogeneous catalyst ink. Then, the ink (4.0 μL) was slowly added onto the surface of glassy carbon electrode as the working electrode and dried at room temperature for 2 h.

4. Electrochemical Measurements

To eliminate the possible interference of N-containing pollutants, the reaction device was repeatedly cleaned with deionized water. There are no other sources of pollution in the testing environment. Before the catalytic measurement, the electrolyte was continually purged with high-purity Ar for 30 min. The electrocatalytic performance was evaluated in an H-type two-compartment cell equipped with a N117 Nafion membrane at room temperature and atmospheric pressure. The membrane was pretreated as follows: It was firstly treated in 5.0 wt% H_2O_2 aqueous solution at 80°C for 1 h and deionized water for 0.5 h. This membrane was immersed in a 5.0 wt% H_2SO_4 aqueous solution at 80°C for 1 h and deionized water for 0.5 h under ambient temperature, respectively. The three-electrode system includes the various materials-modified working electrode, the Hg_2Cl_2/Hg reference electrode and the Pt plate counter electrode, respectively. The Ar-saturated electrolyte contains Na_2SO_4 (0.5 mol L^{-1}) and $NaNO_3$ (0.1 mol L^{-1}). The NO_3RR tests were carried out at different applied potentials, including -1.6, -1.7, -1.8, -1.9 and -2.0 V vs. SCE for 2 h. The cathode electrolyte after electrolysis was analyzed by UV-vis spectra.

5. Detection of Ammonia

Nessler′s reagent approach was used to detect ammonia.[3] Potassium sodium tartrate solution (400 μL, 0.2 M) was added into the diluted post-electrolysis electrolyte (4 mL). The solution was mixed with 400 μL Nessler′s reagent and kept in dark for 20 min to collect the UV-vis absorption spectra. The concentration-absorbance calibration curve was established using a series of standard concentration NH_4Cl solutions and their absorbance values at λ = 425 nm.

In addition, indophenol blue method was applied to estimate the concentration of ammonia.[4] Solution A is 1 M NaOH solution containing 5 wt% salicylic acid and 5 wt% sodium citrate. Solution B is 0.2 M NaClO. Solution C is 1 wt% $C_5FeN_6Na_2O$ (sodium nitroferricyanide) aqueous solution. The diluted post-tested electrolyte (2 mL) was sequentially added by 2 mL solution A, 1 mL solution B and 0.2 mL solution C, which was kept at room temperature for 2 h to correct the UV-vis absorption spectra. The concentration-absorbance curve was calibrated by using a series of standard NH_4Cl solutions and the absorbance intensity at 655 nm. The yield of ammonia can be calculated using the standard curve.

6. Detection of Nitrite

Reagent A is obtained by dissolving sulfanilamide (0.5 g) in 50 mL HCl aqueous solution (2 mol L^{-1}). Another reagent B is prepared by dissolving N-(1-Naphthyl) ethylenediamine dihydrochloride (20 mg) in deionized water (20 mL). The electrolyte (5.0 mL) after NO_3RR was mixed with 0.1 mL reagent A for 10 min. Reagent B (0.1 mL) was further introduced into the above solution, which was allowed to stand for 30 min. The linear relationship was estimated using the UV-vis absorbance intensity at 540 nm and the nitrites (NO_2^-) concentration from standard $NaNO_2$. The NO_2^- concentration was calculated using UV-vis spectra.

7. Detection of Hydrazine

The Watt ad Chrisp method was used to confirm the concentration of hydrazine (N_2H_4).[5] The color reagent was prepared by mixing para-(dimethylamino) benzaldehyde (4 g), concentrated HCl (20 mL) and ethanol (200 mL). The reaction solution (5 mL) after electrocatalysis was mixed with the color reagent (5 mL). The mixture was allowed to stand for 15 min. The UV-vis absorbance at λ = 458 nm was collected to obtain the concentration-absorbance curve by the standard N_2H_4 solution.

8. Calculation of Ammonia Yield Rate and Faradaic Efficiency

The Faradaic efficiency for NO_3RR was defined as the amount of electric charge used for synthesizing NH_3 divided by the total electric charge passing through the electrodes during electrolysis. The total amount of NH_3 was measured by colorimetric methods. Assuming eight electrons were required to produce one NH_3 molecule, the Faradaic efficiency could be calculated as:

$$Faradaic\ efficiency = \frac{8 \times F \times c_{NH_3} \times V}{Q} \times 100\%$$

The ammonia yield rate (R_{NH_3}) was calculated by the following equation:

$$R_{NH_3} = \frac{c_{NH_3} \times V}{t \times S}$$

in which F is the Faraday constant, c_{NH_3} is the measured ammonia concentration, V is the volume of electrolyte, Q is the total charge, t is the electrolysis time, and S is the area of glassy carbon electrode.

9. Isotope Labeling Experiments

The ^{14}N and ^{15}N isotopic experiments were performed by using $Na^{14}NO_3$ and $Na^{15}NO_3$ as raw materials for NO_3RR electrolyte contains Na_2SO_4 (1.0 mol L^{-1}) and $Na^{14/15}NO_3$ (0.1 mol L^{-1}) at -1.9 V vs. SCE for 2 h. For quantitative ^1H NMR measurements, various concentrations of ammonium chloride were used to prepare the standard curves. The post electrolyte (1 mL) was mixed with H_2SO_4 (1 mL, 0.1 M) and DMSO-d_6 solutions (0.2 mL), which was used for ^1H NMR measurement.

10. Computational Details

Geometries of materials were optimized using the Gaussian 16 C.01 software at the PBE1PBE-D3(BJ)/6-31+G* level of theory.[6,7] In calculating the free energy, the free energy contributions of protons and electrons were accounted for using the computational hydrogen electrode (CHE) method.[8,9]

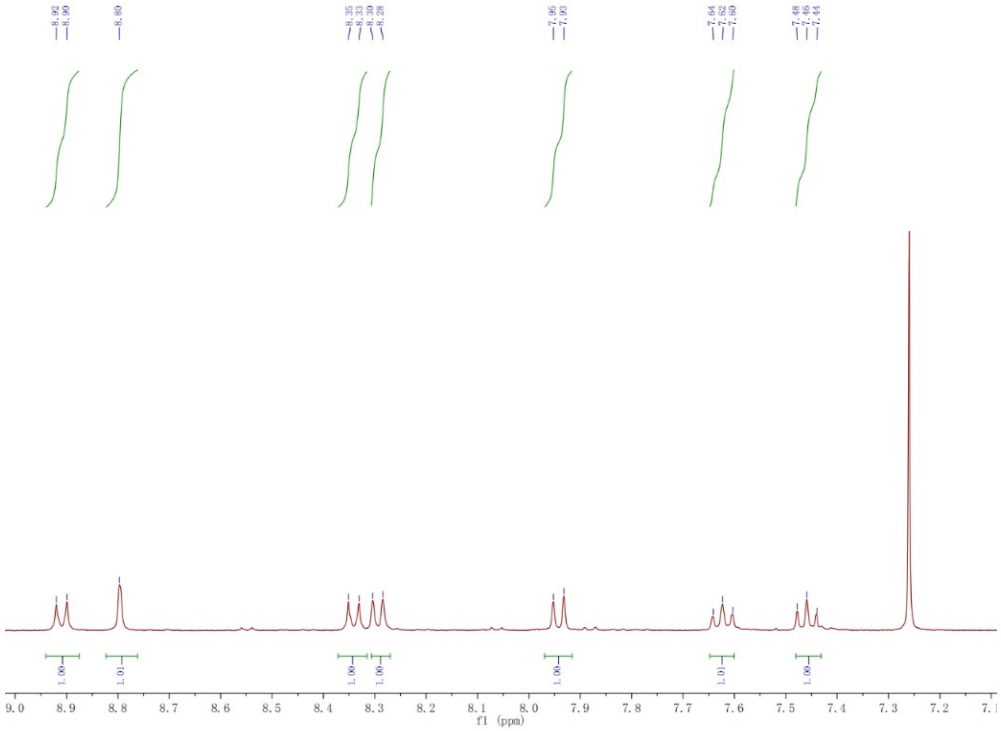

Fig. S1. ^{1}H NMR spectrum of TCPP in $CDCl_3$.

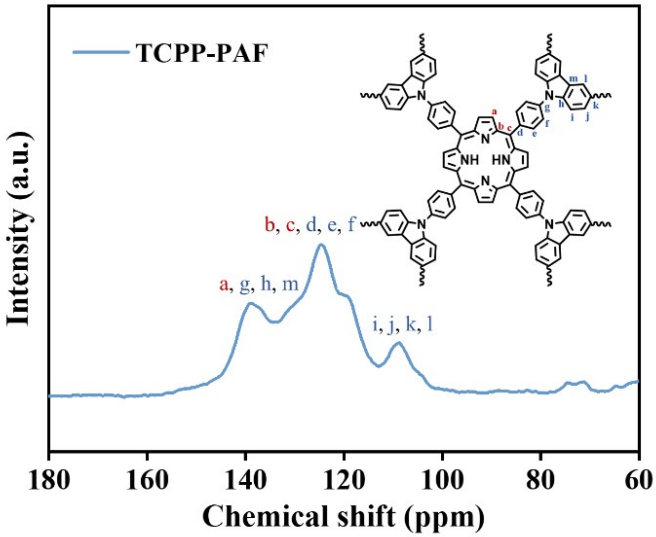

Fig. S2. The solid-state ^{13}C NMR spectrum of TCPP-PAF.

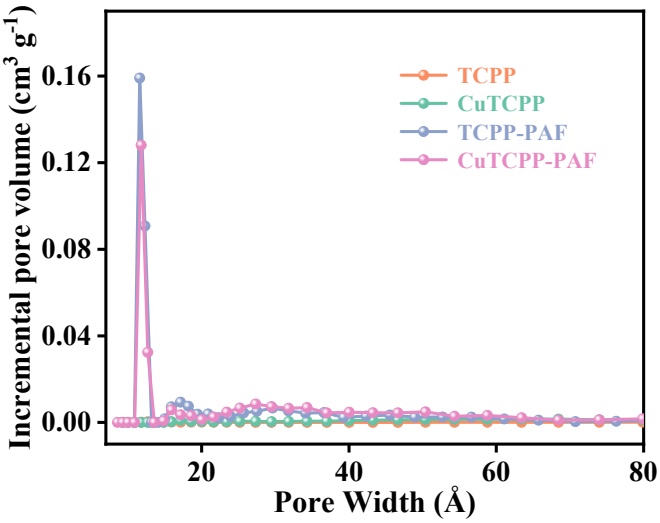

Fig. S3 Pore size distributions of TCPP, CuTCPP, TCPP-PAF and CuTCPP-PAF.

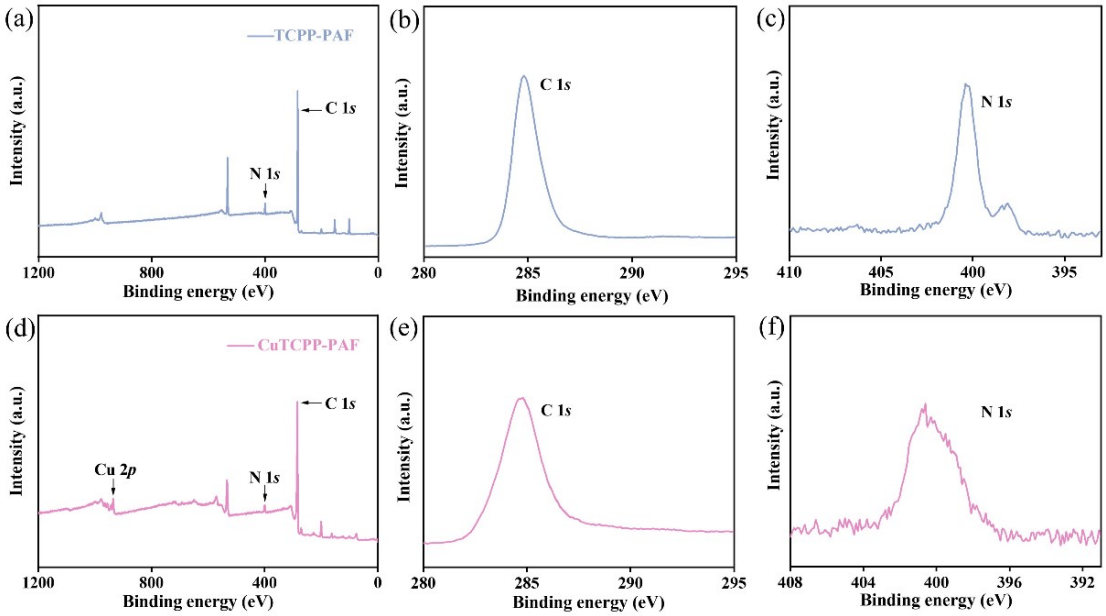

Fig. S4 Full XPS spectra of (a) TCPP-PAF and (d) CuTCPP-PAF. High-resolution C 1*s* and N 1*s* XPS of (b, c) TCPP-PAF and (e, f) CuTCPP-PAF.

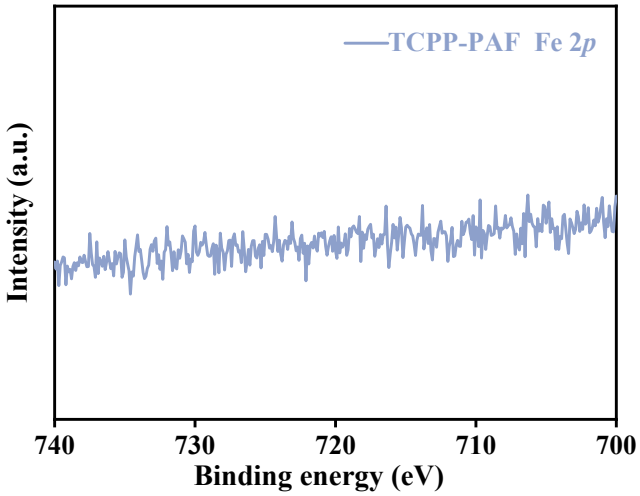

Fig. S5 High-resolution Fe 2*p* XPS of TCPP-PAF.

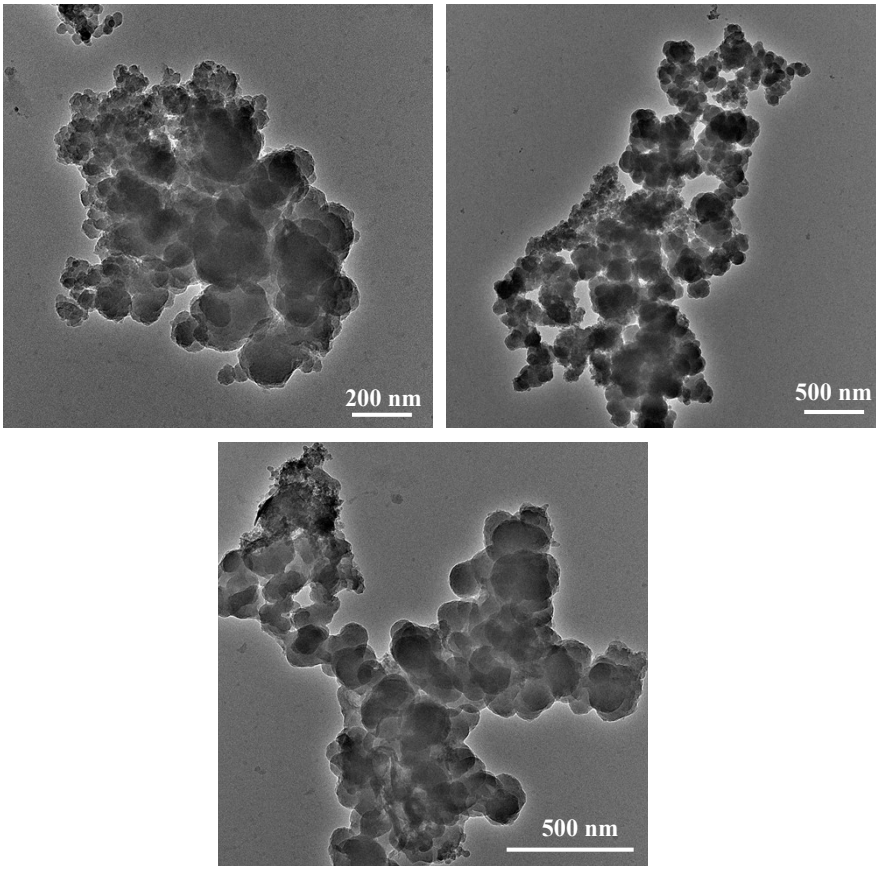

Fig. S6 The TEM images of CuTCPP-PAF.

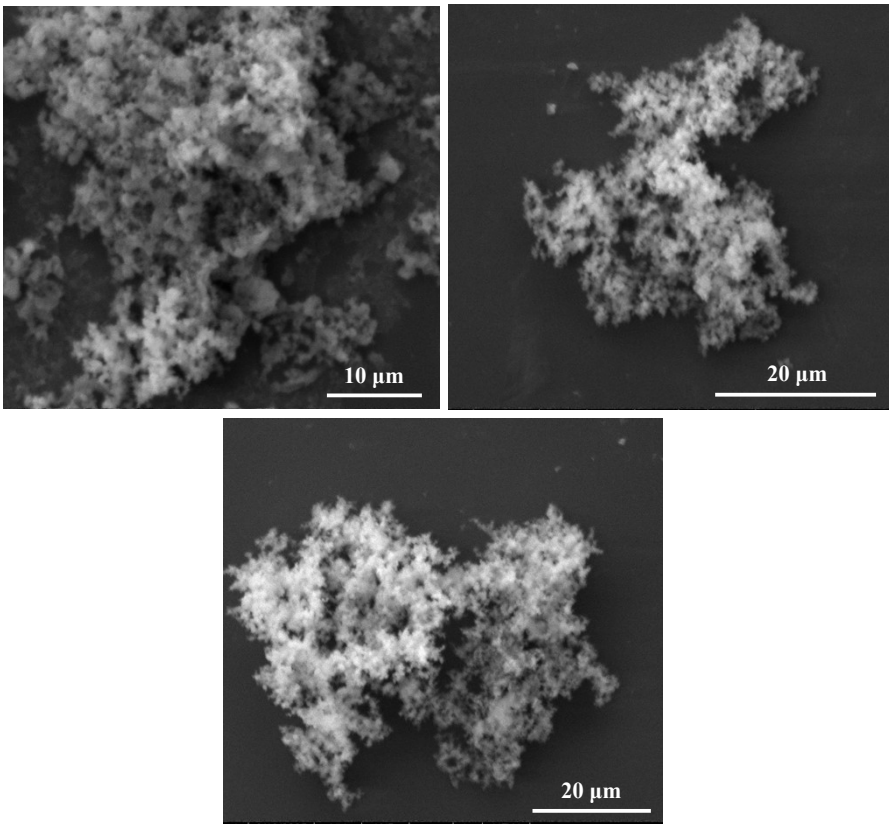

Fig. S7 The SEM images of CuTCPP-PAF.

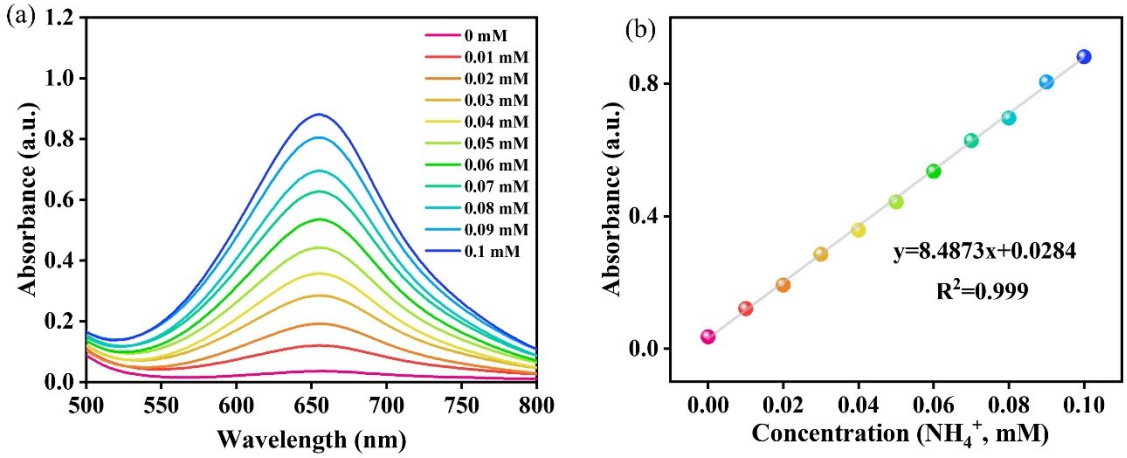

Fig. S8 (a) UV-vis curves of indophenol blue solutions. (b) Calibration curve used for the estimation of NH_4^+ concentration.

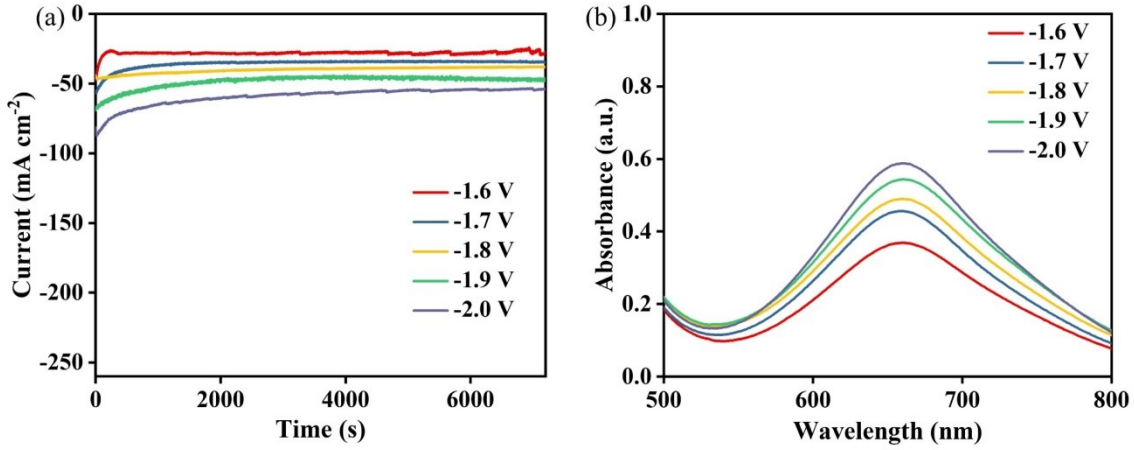

Fig. S9 (a) CA curves and (b) UV-vis spectra of electrolytes after electrocatalytic NO_3RR at different potentials using CuTCPP-PAF.

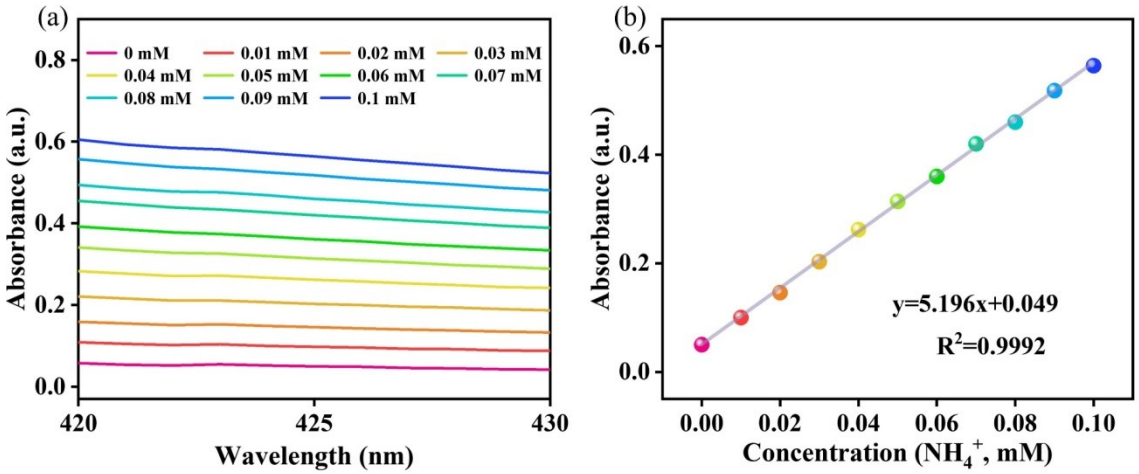

Fig. S10 (a) UV-vis curves of Nessler's reagent solutions. (b) Calibration curve used for the estimation of NH_4^+ concentration.

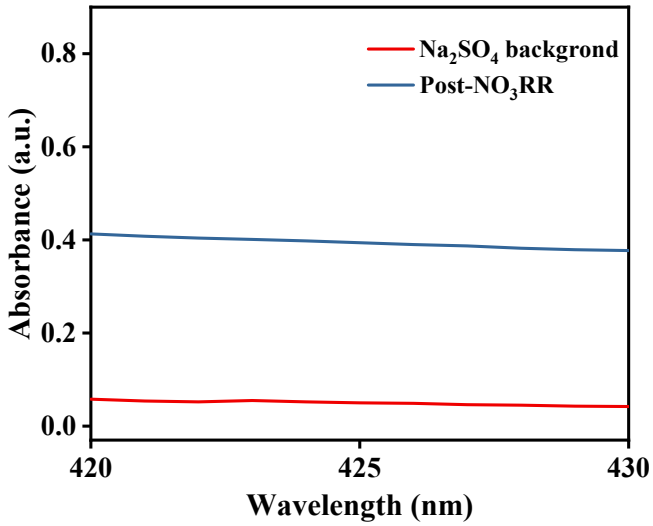

Fig. S11 (a) UV-vis spectra of Nessler's reagent solutions after electrocatalytic NO_3RR at -1.9 V vs. SCE using CuTCPP-PAF.

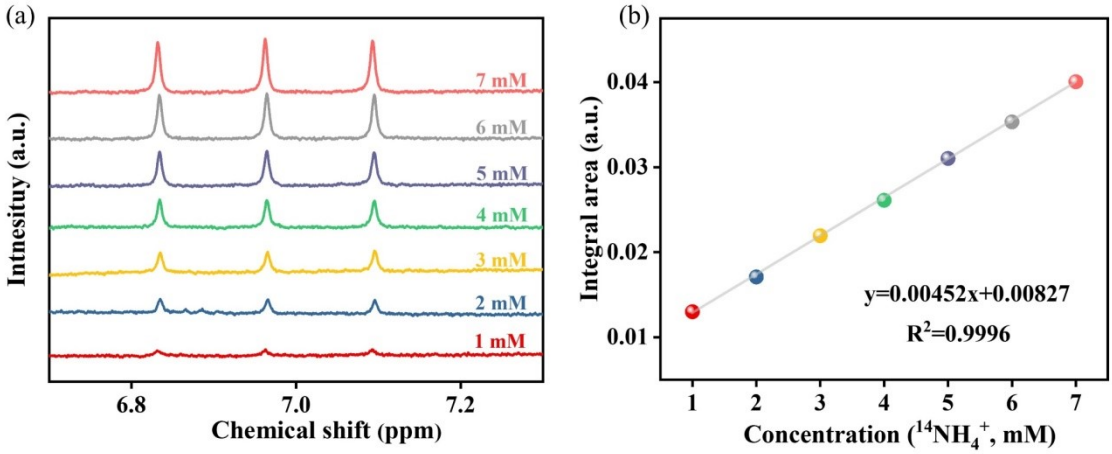

Fig. S12 (a) ^{1}H NMR spectra of $^{14}NH_4^+$ solutions. (b) The calibration curve used for the estimation of the $^{14}NH_4^+$ concentration.

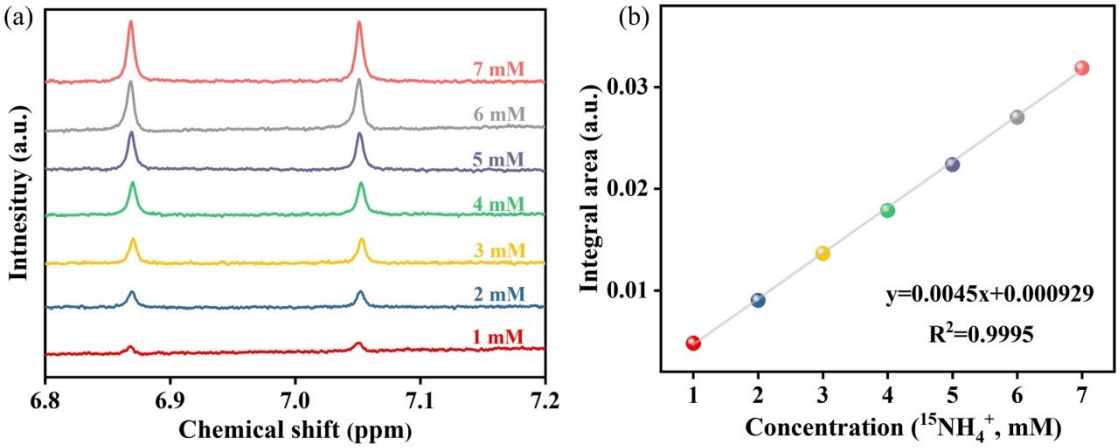

Fig. S13 (a) ^{1}H NMR spectra of $^{15}NH_4^+$ solutions. (b) The calibration curve used for the estimation of the $^{15}NH_4^+$ concentration.

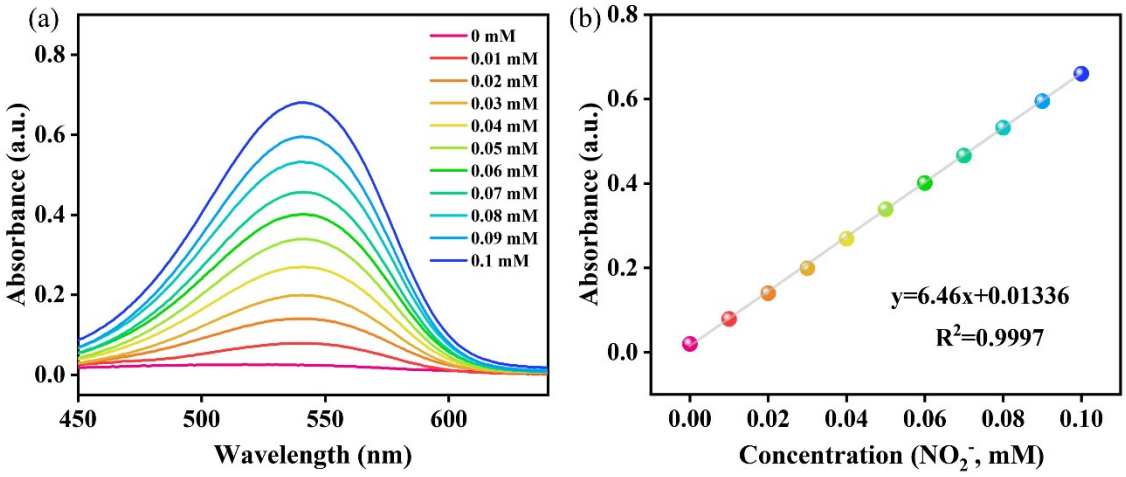

Fig. S14 (a) UV-vis curves and (b) calibration curve used for the estimation of NO_2^- concentration.

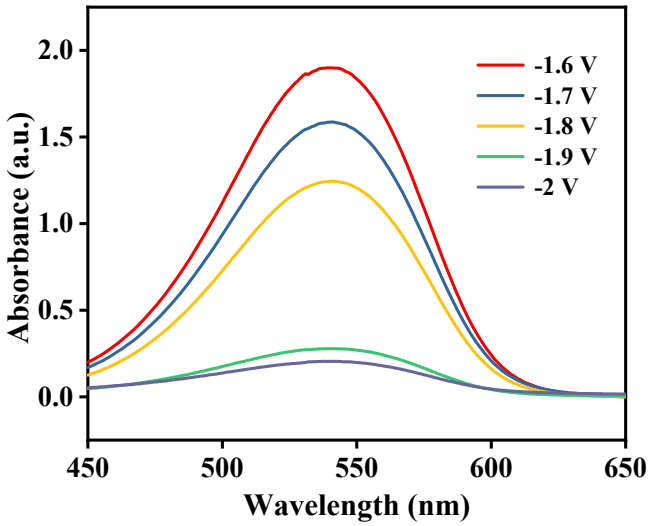

Fig. S15 UV-vis spectra of the NO_2^- concentration after electrocatalytic NO_3RR using CuTCPP-PAF.

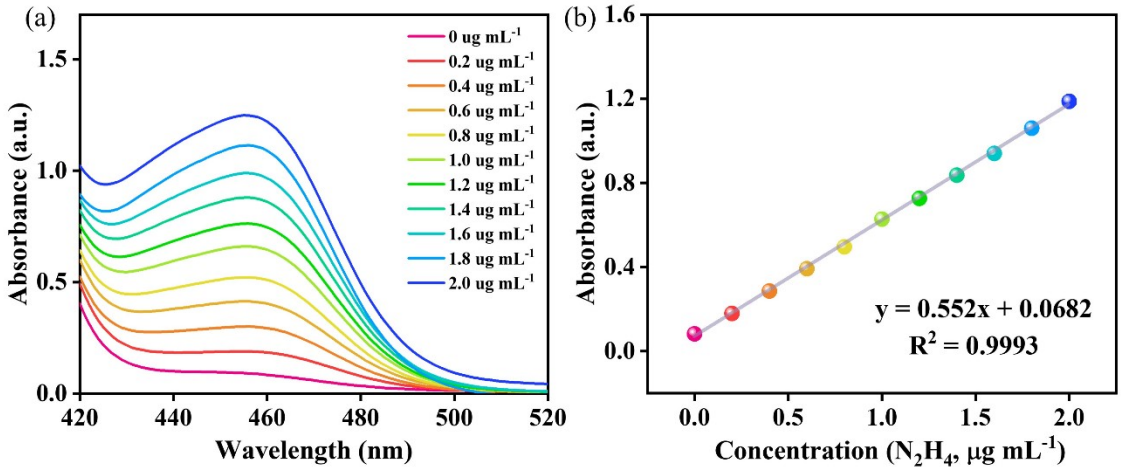

Fig. S16 (a) UV-vis absorption spectra and (b) the calibration curve for the quantification estimation of N_2H_4 concentration.

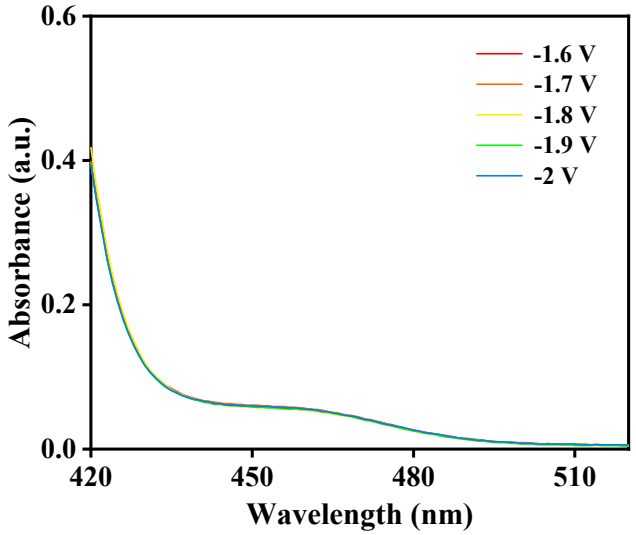

Fig. S17 UV-vis absorption spectra of the hydrazine concentration during electrocatalytic NO_3RR at various applied potentials using CuTCPP-PAF.

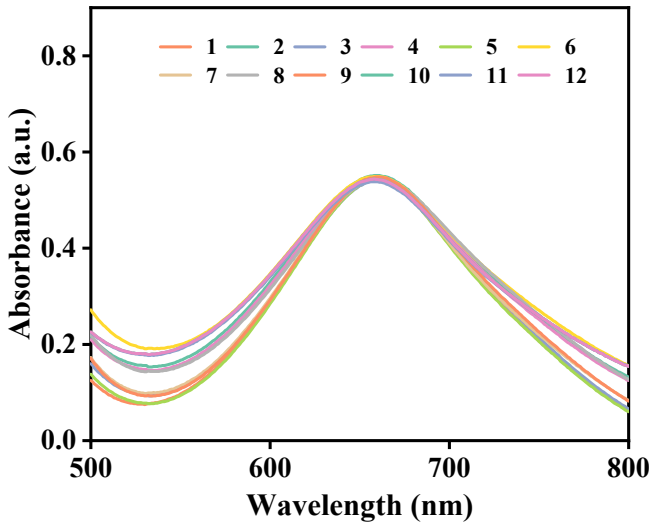

Fig. S18 UV-vis spectra of electrolytes after electrocatalytic NO_3RR at -1.9 V vs. SCE using CuTCPP-PAF for twelve cycles.

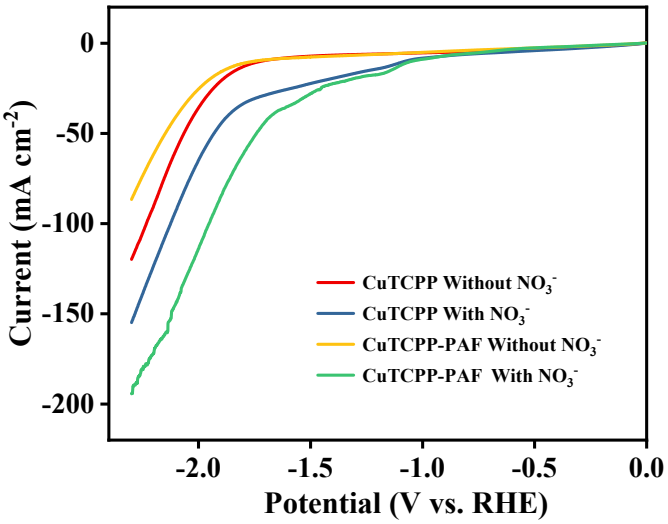

Fig. S19 LSV curves in 0.5 M Na_2SO_4 with and without 0.1 M NO_3^- of CuTCPP and CuTCPP-PAF.

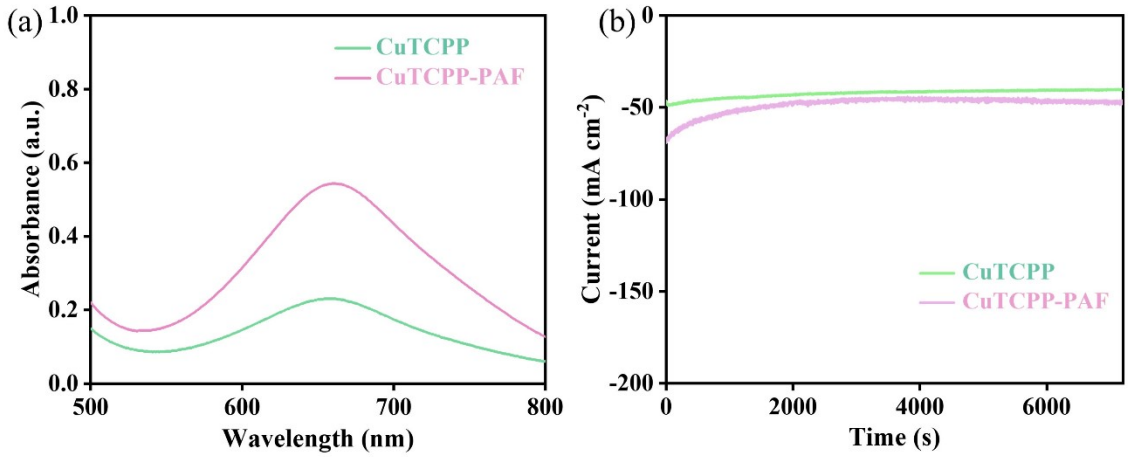

Fig. S20 (a) UV-vis spectra and (b) CA curves of electrolytes after electrocatalytic NO_3RR at -1.9 V vs. SCE for 2 h.

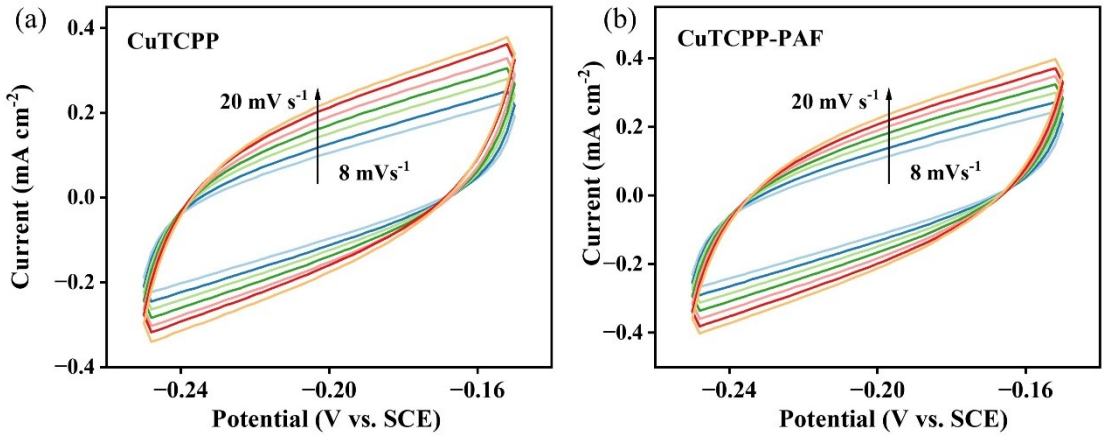

Fig. S21 CV curves at various scan rates of (a) CuTCPP and (b) CuTCPP-PAF.

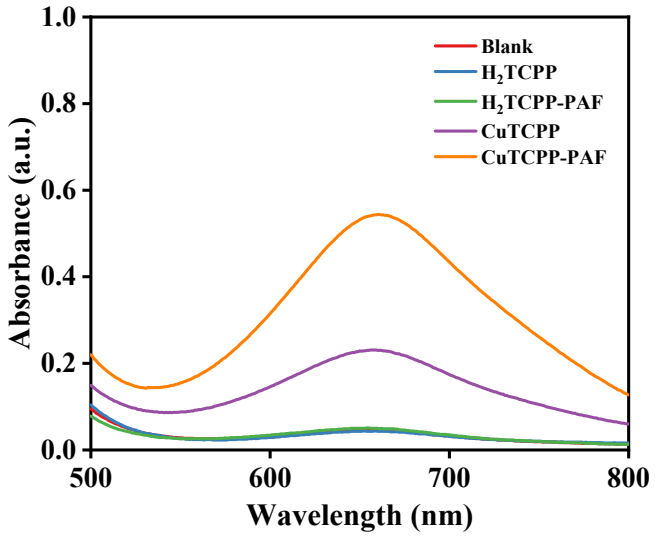

Fig. S22 UV-vis spectra of the blank electrolyte, H_2TCPP, H_2TCPP-PAF, CuTCPP, and CuTCPP-PAF after electrocatalytic NO_3RR at -1.9 V vs. SCE for 2 h.

Table S1 Different materials for electrocatalytic NO_3RR.

Material	Electrode type	Electrolyte	Optimal potential	NH_3 yield ($mg\ h^{-1}cm^{-2}$)	FE (%)	Ref.
NiFe-LDH	3 × 3 cm^2 $FeNi_x$/FF	200 mg L^{-1} NO_3^-	−1.1 V vs. Ag/AgCl	0.21	65.2	[10]
Ni-MOFNF	1 × 3 cm^2 Ni-MOF/NF	70 mg L^{-1} NO_3^-	−1.4 V vs. SCE	1.87	80	[11]
Ce MOF-Cu	1 × 1 cm^2 carbon cloth	5 mM $NaNO_3$	−0.9 V vs. RHE	1.12	85.5	[12]
NiPr-TPA-COF	1 × 1 cm^2 carbon paper	0.1 M KNO_3	−1.38 V vs. SCE	2.5	90	[13]
RuFe-FeNC	1 × 1 cm^2 carbon paper	0.1 M KNO_3	−1.4 V vs. RHE	0.012	92.2	[14]
CuNi-LDHs	0.5 × 0.5 cm^2 carbon paper	0.1 M KNO_3	−0.4 V vs. RHE	2.73	94.6	[15]
Co-B@CoO_x	Co-B@CoO_x on Ni foam	100 ppm NO_3^-	−0.9 V vs. RHE	1.69	95.72	[16]
Cu@CuHHTP	1 × 1 cm^2 carbon paper	500 ppm NO_3^-	−0.9 V vs. RHE	1.84	96.84	[17]
RuCu	1 × 1 cm^2 carbon paper	0.1 M KNO_3	−0.4 V vs. RHE.	1.63	97.2	[18]
CuTCPP-PAF	glassy carbon electrode	0.1 M $NaNO_3$	−1.9 V vs. SCE	3.6	98.6	This work

References

1. L. J. Feng, Q. Chen, J. H. Zhu, D. P. Liu, Y. C. Zhao and B. H. Han, *Polym. Chem.* 2014, **5**, 3081-3088.
2. Q. Chen, M. Luo, P. Hammershoj, D. Zhou, Y. Han, B. W. Laursen, C. G. Yan and B. H. Han, *J. Am. Chem. Soc.*, 2012, **134**, 6084-6087.

3. Y.C. Hao, Y. Guo, L.W. Chen, M. Shu, X.Y. Wang, T.A. Bu, W.Y. Gao, N. Zhang, X. Su, X. Feng, J.W. Zhou, B. Wang, C.W. Hu, A.X. Yin, R. Si, Y.W. Zhang and C.H. Yan, *Nat. Catal.*, 2019, **2**, 448–456.
4. J. Wang, L. Yu, L. Hu, G. Chen, H. Xin and X. Feng, *Nat. Commun.*, 2018, **9**, 1795.
5. W. Xu, G. Fan, J. Chen, J. Li, L. Zhang, S. Zhu, X. Su, F. Cheng and J. Chen, *Angew. Chem. Int. Ed.*, 2020, **59**, 3511–3516.
6. M. J. Frisch, G. W. Trucks, H. B. Schlegel, et al., Gaussian 16, Revision C.01, Gaussian, Inc., Wallingford CT, 2016.
7. S. Grimme, J. Antony, S. Ehrlich and H. Krieg, *J. Chem. Phys.*, 2010, **132**, 154104.
8. R. Dronskowski and P. E. Blöchl, *J. Phys. Chem.*, 1993, **97**, 8617–8624.
9. V. L. Deringer, A. L. Tchougréeff and R. Dronskowski, *J. Phys. Chem. A*, 2011, **115**, 5461–5466.
10. K. Wang, R. Mao, R. Liu, J. Zhang, H. Zhao, W. Ran and X. Zhao, *Nat. water,* 2023, **1**, 1068–1078.
11. F. Pan, J. Zhou, T. Wang, Y. Zhu, H. Ma, J. Niu and C. Wang, *J. Colloid. Interf. Sci.,* 2023, **638**, 26-38.
12. Y. Xu, M. Xie, H. Zhong and Y. Cao, *ACS Catal.*, 2022, **12**, 8698−8706.
13. F. Lv, M. Sun, Y. Hu, J. Xu, W. Huang and N. Han, *Energy Environ. Sci.*, 2023, **16**, 201-209.
14. X. Zhao, Y. Jiang, M. Wang, S. Liu, Z. Wang, T. Qian and C. Yan, *Adv. Energy Mater.,* 2023, **13**, 2301409.
15. H. Li, S. Li, R. Guan, Z. Jin, D.an Xiao, Y. Guo and P. Li, *ACS Catal.*, 2024, **14**, 12042−12050.
16. X. Zhu, C. Ma, Y. Wang, K. Qu, L. Song, J. Wang, Y. Gong, X. Liu, J. Zhang, Q. Lu and A. Wang, *Energy Environ. Sci.,* 2024, **17**, 2908.

17. X. Zhu, H. Huang, H. Zhang, Y. Zhang, P. Shi, K. Qu, S. Cheng, An. Wang and Q. Lu, *ACS Appl. Mater. Interfaces*, 2022, **14**, 32176−32182.

18. K. Liu, Z. Sun, X. Peng, X. Liu, X. Zhang, B. Zhou, K. Yu, Z. Chen, Q. Zhou, F. Zhang, Y. Wang, X. Gao, W. Chen and P. Chen, *Nat. Commun.*, 2025, **16**, 2167.